Molecular dynamics study of the configurational and energetic properties of the silicon self-interstitial

Luis A. Marqués, Lourdes Pelaz, Pedro Castrillo, and Juan Barbolla
Departamento de Electrónica, Universidad de Valladolid, E.T.S.I. de Telecomunicación, 47011 Valladolid, Spain
(Received 7 October 2004; revised manuscript received 17 November 2004; published 17 February 2005)

We have carried out classical molecular dynamics simulations to study the configurational and energetic properties of the Si self-interstitial. We have shown that the Si self-interstitial can appear in four different configurations, characterized by different energetics. Along with the already known tetrahedral, dumbbell, and extended configurations, we have found a highly asymmetric configuration not previously reported in the literature. Using a data analysis technique based on time averages, we have extracted the formation enthalpies and the probability of finding the interstitial in a given configuration, both depending on temperature. By the use of thermodynamic integration techniques we have determined the Gibbs free energy and entropy of formation, and the relative concentration of each interstitial configuration as a function of temperature. We have demonstrated that the change of interstitial configuration is correlated with the diffusion process, and we have identified two different mechanisms for interstitial-mediated self-diffusion. In spite of the microscopic complexity of the interstitial-mediated diffusion process, our results predict a pure Arrhenius behavior with an activation energy of 4.60 eV in the temperature interval 900–1685 K, in good agreement with experiments. This energy is decomposed in an effective interstitial formation enthalpy of 3.83 eV and a migration barrier of 0.77 eV, which macroscopically represent the averaged behavior of the different interstitial configurations.

DOI: 10.1103/PhysRevB.71.085204 PACS number(s): 61.72.Ji, 61.72.Bb, 66.30.Fq

I. INTRODUCTION

Native point defects in Si, vacancies and self-interstitials, have been an important field of both theoretical and experimental research for several decades. The interest in its study continues today due to their role in a large variety of phenomena, especially in those related to the fabrication of microelectronic devices. Native Si defects affect the microstructure evolution of the material during several of the IC manufacturing steps, and thus can alter the final performance of the device.[1] Understanding their behavior and properties is important in order to develop predictive atomistic simulators for the design of new IC generations by saving the realization of expensive and time-consuming test lots.[2]

The study of the Si self-interstitial properties is of particular importance. Self-interstitials have been implicated as the origin of rodlike defects observed in Czochralski single-crystal growth, which can ultimately produce the degradation of the manufactured ultralarge-scale integrated silicon devices.[3] On the other hand, during the implantation step a large concentration of interstitials is introduced in the lattice. Upon subsequent annealing at elevated temperatures these interstitials interact with dopants, such as B, and cause the so-called *transient-enhanced diffusion*, which alters the junction depth.[4] This effect is becoming more and more critical as the size of devices shrinks on every new IC generation. Besides, Si self-interstitials have also been given a role in the understanding of amorphous phase formation.[5,6]

In spite of the great number of studies devoted to it, the interstitial contribution to Si self-diffusion is far from being fully understood. Experiments have established that Si self-diffusion obeys an Arrhenius behavior over a wide range of temperatures with an activation energy of 4.5–4.8 eV.[7–10] The self-diffusivity D_{SD} is written as the sum of contributions from independent diffusive mechanisms or defects, $D_{SD}=\Sigma_i D_i C_i$, where D_i and C_i are the diffusivity and concentration, respectively, of the relevant defect. Only two diffusive mechanisms are routinely considered in Si: the vacancy-mediated and the self-interstitial-mediated diffusion mechanisms. A third one, the concerted exchange of Pandey,[11] is based on the defect known as *IV pair* or simply *bond defect*, which consist of a local distortion of the Si lattice with no excess of deficit of atoms.[12,13] It is a low formation energy defect that maintains fourfold coordination. Even though it has been given a fundamental role in the Si amorphization process,[14,15] its contribution to diffusion is usually disregarded[9] since it has been theoretically demonstrated to be negligible in comparison to the other two mechanisms.[16] Even though the Si self-diffusion process is well characterized experimentally, the individual contributions to it from vacancies and self-interstitials are still an open question, as well as the determination of D_i and C_i. Usually additional hypotheses have to be introduced since direct experimental detection of Si self-interstitials has proved to be difficult.[1]

In order to complement these experiments, theoretical studies have been carried out to determine the configuration and energetics of the Si self-interstitial, as well as its diffusive behavior. These include first principles,[13,16–21,23] tight binding (TB),[12,24–29] and classical potential calculations.[5,6,30–38] However, even when using the same calculation techniques, different authors come to different conclusions regarding the Si self-interstitial properties. The discrepancies are mainly related to the determination of the lowest formation energy configuration and to the microscopic description of the interstitial-mediated self-diffusion mechanism.

Most of the first-principle studies of the Si self-interstitial properties are based on static minimization techniques,

mainly because of the limitation on the simulation times ($<$30 ps) that can be treated. Statical minimization techniques have been shown to give useful information, above all those related to defect formation energies. However, with its use the system could get trapped in a local potential minimum instead of finding the global one. Sometimes, defect configurations obtained by statical methods have been shown to be unstable.[21] Symmetry is often enforced when searching possible configurations and migration paths, and that can occasionally lead to wrong conclusions.[14,21] These limitations, which could explain the discrepancies among results of different authors, would be avoided by using fully dynamical simulations. However, that is not possible within the first-principle framework due to the excessive computational workload, except for temperatures close to the Si melting point.[16] Unfortunately, to be able to do fully dynamical simulations it is necessary to resort to empirical approaches, at the expense of losing the "parameter-free" character of the first-principle methods. In fact, to get reliable statistics on the different interstitial configurations (several thousands of samples) and to accurately describe the diffusion process (several hundreds of diffusion hops) at intermediate temperatures (around 1000 K), even the TB technique could be computationally prohibitive. Classical potentials allow us to afford such kinds of long dynamical simulations, but the electronic description of the system is lost and some care has to be taken in order to extrapolate results to situations not explicitly included in the potential parameter-fitting process. In the literature, the vast majority of classical studies on the Si self-interstitial have been carried out using the Stillinger-Weber (SW) potential,[39] and consequently their properties within the SW description are rather well established. This is not the case for the Tersoff potential.[40]

In this paper we present a thorough study of the Si self-interstitial configurational and energetic properties using molecular dynamics (MD) calculations within the Tersoff description. The MD technique is briefly introduced in Sec. II, as well as the motivations behind the use of the Tersoff potential and the particular conditions of our calculations. In order to analyze the simulation data, we used a technique based on time averages of atom coordinates along the simulation, which is presented in Sec. III and compared with other analysis methods routinely used. In Sec. IV the main results of our work are presented, with special emphasis on the comparison with results obtained by other authors using different techniques, both theoretical and experimental. Finally, in Sec. V some conclusions are drawn.

II. MOLECULAR DYNAMICS SIMULATIONS

The MD simulation technique consists of the numerical resolution of the equations of motion for a system of N atoms.[41] These equations are discretized in time and solved in a computer by using a suitable integration algorithm. The outcome of the MD simulation in each time step Δt is the set of positions $\vec{r}^N$ and momenta $\vec{p}^N$ for all atoms. The phase-space trajectory of the system can be represented by the set of numbers:

$$\{[\vec{r}^N(k\Delta t),\vec{p}^N(k\Delta t)], \quad k=1,\ldots,M\}, \tag{1}$$

where M is the total number of discrete points needed to cover a given simulation time t ($t=M\Delta t$). From the computed trajectory it is possible to extract the average of a system property A by

$$\langle A\rangle = \frac{1}{M}\sum_{k=1}^{M} A[\vec{r}^N(k\Delta t),\vec{p}^N(k\Delta t)], \tag{2}$$

provided the relation between A and $\vec{r}^N$ and $\vec{p}^N$ is known and the total simulation time t is long enough.

In the MD technique the interactions among the atoms determine the system dynamics. Consequently, it is important to use interatomic potentials that represent as close as possible the interactions in the real material. In our study, even though no large systems are necessary, we have to simulate very long times, at least for the lower temperatures. We resorted to the use of an empirical interatomic potential, much less computationally intensive than first-principles or TB methods. Among the several potentials for Si that can be found in the literature (see Ref. 42 for a comparative study), we have chosen to use the one developed by Tersoff within its third parametrization (T3).[40] It takes into account many-body interactions through the use of an effective coordination term that depends on the bond lengths and their relative orientations. The potential parameters were fitted to a database consisting of cohesive energies of real and hypothetical (obtained by *ab initio* methods) bulk polytypes of Si, along with the bulk modulus and bond length in the diamond structure. In addition, the potential was required to reproduce all three elastic constants of Si to within about 20%. Even though no point defect data were included in the fitting process, the fact that data regarding structures not having fourfold coordination were used in the fitting suggests that the T3 potential could be more suitable than others at describing point defects, since the involved atoms are also not fourfold coordinated. In fact, Tersoff compared the point defect energies predicted by T3 with first-principle calculations showing that values were consistent within 1–2 eV,[40] which was only a factor of 2 worse than the consistency among the *ab initio* results of different groups.

A limitation attributed to the T3 potential is that it predicts a melting point temperature for Si of around 2400 K,[14] well above the value found in the experiments, 1685 K.[43] This is not an important drawback since it is possible to make a rescaling between real and T3 temperatures. Porter *et al.* related the simulation temperature T_{T3} with a scaled real temperature T_{real} by requiring that the internal energy of the classical simulation system at T_{T3} be equal to that of a corresponding quantum system at T_{real}.[44] They defined a temperature scaling expression based on a fifth-order polynomial that related T_{T3} with T_{real}. Unfortunately, their scaling law only comprised the temperature range up to $T_{real}=700$ K. Since our simulations have been carried at higher temperatures, we have extrapolated their scaling law with a second-order polynomial. We have fitted the polynomial parameters by assuring continuity of the scaling law and its first derivative at $T_{real}=700$ K, and making the real melting temperature

of 1685 K coincident with the T3 melting temperature of 2400 K. The resulting scaling law is given by

$$T_{T3} = 6.95 \times 10^{-4} T_{real}^2 + 2.66 \times 10^{-2} T_{real} + 3.79 \times 10^2, \tag{3}$$

where both T_{T3} and T_{real} are in K. In the following temperature T will be taken to mean T_{real}, as given by Eq. (3), unless otherwise noted.

In spite of being one of the most used Si empirical potentials in MD calculations, there are few studies on the Si self-interstitial properties within the T3 description. Ungar *et al.* used the T3 potential to study free energies, structures and diffusion of point defects in Si,[33] in order to complete a previous study carried out by Balamane and co-workers.[42] However, instead of carrying out dynamic simulations, they used the Monte Carlo (MC) framework, and in the case of the self-interstitial they only considered one possible configuration. Nevertheless, they found that the T3 potential gives a fairly good description of the point defect formation and migration energies. On the other hand, in a recent work Nishihira and Motooka observed the generation and movement of interstitial defects from a planar crystal-amorphous interface.[38] They used MD simulations with the T3 potential. However, their interest was mostly focused on the study of the recrystallization process.

To study the variation of the Si self-interstitial properties with temperature we carried out MD simulations for several temperature values between 900 K and 1685 K. We have used a system consisting of 576 Si atoms, large enough to get reliable values of the formation energies, and more than double the system size of previous MC simulations.[33] The dimensions of the computational cell were $4a \times 3\sqrt{2}a \times 3\sqrt{2}a$, a being the Si basic unit cell length (5.43 Å). The MD cell, of approximately the shape of a cube, was bounded by two (100) planes in the X direction and by four (110) planes in Y and Z directions. To minimize finite size effects we used periodic boundary conditions along the three axes. We solved the classical equations of motion using the fourth-order Gear predictor-corrector algorithm[45] with a variable time step, which is chosen as an inverse function of the maximum kinetic energy E_{Kmax} present in the system:

$$\Delta t = K/\sqrt{E_{Kmax}}, \tag{4}$$

where K is a proportionality constant chosen in such a way that the most energetic particle in the system takes 100 time steps to cover the distance between two consecutive atom planes in the ⟨100⟩ direction. This condition assures total energy conservation.

Initially the atoms are set to occupy perfect lattice positions. An extra atom is then introduced in a hexagonal interstitial position, just to keep it as far as possible from its first neighbors in the perfect lattice (if the extra atom is set close to any host atom, an artificially high repulsive energy may be introduced in the cell). Atom positions are then rescaled to account for thermal expansion in order to keep external pressure close to zero (conveniently then energies are assimilated to enthalpies). Initial velocities are chosen from a Maxwell-Boltzmann distribution corresponding to each temperature to be simulated. Due to the exchange between kinetic and potential energies, it is necessary to rescale atom velocities several times during an initial run to finally equilibrate the system at the desired temperature. Then the system is allowed to freely evolve in the *NVE* ensemble until the total simulation time is reached. This time should be long enough to ensure that a meaningful part of the phase space has been sampled in order to apply Eq. (2). Due to the slower dynamics in the lower temperature range, this total simulation time can be as high as one-tenth of a microsecond.

III. ANALYSIS OF THE SIMULATION DATA

We are interested in the study of the time evolution of the configurational and energetic properties of the Si self-interstitial at different temperatures. Even though MD is a powerful tool to study defect dynamics at an atomistic level, some problems arise when analyzing data directly extracted from the simulations. Usually thermal agitation precludes the direct analysis of configurations and energetics, above all at high temperatures. To get a clean configuration from a MD run, several techniques are routinely used, such as the *cooling down to* 0 K or the *steepest-descent/conjugate-gradient* minimization methods.[5,27,34] In cooling down to 0 K the kinetic energy of the system is slowly drained via velocity rescaling until the total temperature has dropped close to 0 K. In the minimization methods atoms are moved along the direction of the maximum variation of the interatomic potential function. In both cases particles are gradually displaced to their closest local potential minimum, thus eliminating thermal vibrations. Then it is possible to extract clean configurations and formation energies for the defect. However, these techniques are relatively computer demanding, and thus they cannot be applied to every configuration obtained from the MD simulation. Besides, there is no certainty of reaching the global potential minimum instead of a local minimum.

On the other hand, to get the diffusion path and the transition state between two different configurations it is necessary to use relatively complex techniques such as the *nudged elastic band method*,[46] the *discretized path optimization*,[47] or the *eigenvector-following approach*.[27] Reaction paths describe the lowest-energy path connecting two defect configurations. The highest-energy point on this path, or *saddle point*, determines the energy barrier for the transition between those two configurations. However, the cited methods usually require knowledge of both the initial and final configurations *a priori*, as well as a guess of the overall reaction path.[36,48]

To analyze the data from the MD simulations we have used a very simple method that overcomes the mentioned drawbacks. It is based on the time average of the atom coordinates, and it has been successfully used to study recrystallization processes in Si.[49,50] Figure 1 serves to illustrate the effectiveness of the scheme. Solid lines represent the projection in the XY plane of the trajectories followed by seven atoms (the Si self-interstitial and its six closest neighbors) during 1000 steps in a MD simulation carried out at 1600 K. As can be seen, each atom vibrates around the corresponding

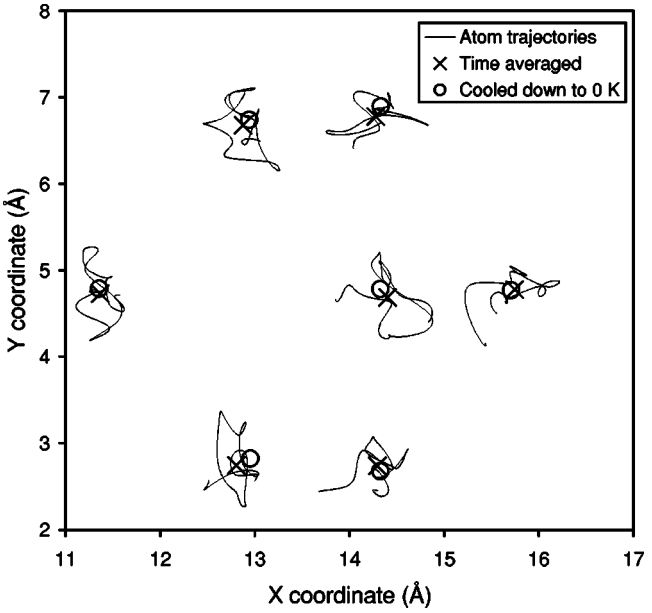

FIG. 1. *XY* projection of the trajectories followed by a Si self-interstitial and its neighbors during 1000 simulation steps at 1600 K. Open circles represent the potential energy minima, as obtained by cooling down to 0 K. Crosses arethe positions obtained by time averaging the atom coordinates during the 1000 steps.

local potential energy minimum. It is clear how these vibrations preclude the direct determination of the configurational and energetic properties of the Si self-interstitial, above all at high temperatures such as 1600 K. The result of the time average during 1000 simulation steps, and the atom coordinates obtained by cooling down to 0 K using atom velocity rescaling every 1000 steps for a total MD simulation run of 10^6 steps, are also represented in the figure. As it can be seen, time averaging gives a very good approximation to the positions obtained by cooling down to 0 K, but at a much lesser computational cost. Besides, this technique can be applied *on the fly*, i.e., during the actual MD simulation. Consequently, it allows us to extract the evolution in time of the Si self-interstitial configuration and energetics. Saddle points appear in a natural way as intermediate configurations during Si self-interstitial diffusion, as we shall see in the next section.

For each simulated temperature, we have carried out time averages for 1000 steps. The temperature is proportional to the total kinetic energy of the system.[41] Considering Eq. (4), it is clear that the time step will be shorter for higher temperatures. Consequently, 1000 simulation steps are equivalent in terms of system dynamics for any temperature, since the enhanced particle mobility at high temperatures is compensated by shorter time steps. Each averaged configuration is compared to the perfect lattice at each temperature. When an atom is closer than 0.7 Å to a lattice site, the atom is associated with that site; otherwise it is labeled as *displaced*. In the same way, lattice sites with no associated atom are labeled as *empty*. This method allows a first classification of the Si self-interstitial configurations. When different configurations share the same number of displaced atoms and empty sites, the classification can be easily done taking into account

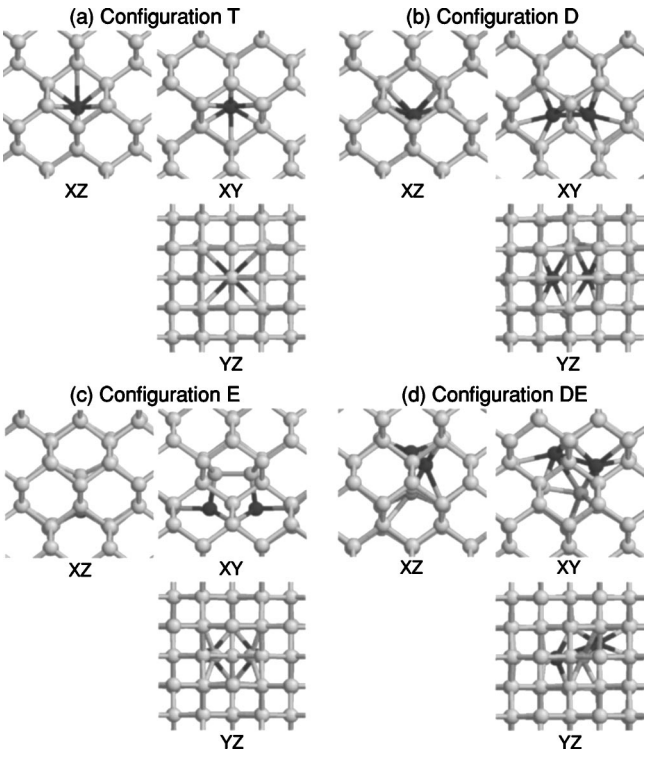

FIG. 2. *XY*, *XZ*, and *YZ* projections of the different Si self-interstitial configurations found in our simulations. Gray scale represents potential energies, where darker tones correspond to higher values.

geometrical considerations (distances between displaced atoms or between displaced atoms and empty sites).

IV. RESULTS AND DISCUSSION

A. Si self-interstitial configurations and energetics

Once each set of averaged atomic positions obtained along the simulation is classified in terms of displaced atoms and empty sites, we have made an statistical study of the morphology and energetics of each interstitial configuration. We have identified four basic configurations, which are shown in Fig. 2. In the first one, there are no empty lattice sites but one displaced atom which occupies a tetrahedral interstitial site. This is the so-called *tetrahedral interstitial*, usually represented by T. Figure 2(b) shows the *dumbbell interstitial* (D), where two displaced atoms oriented along the ⟨110⟩ direction share a common lattice site. T and D interstitials are the most studied Si self-interstitial configurations.[12,30,32,33,51] In Fig. 2(c) appears the *extended interstitial* (E), which consists of four displaced atoms and three empty lattice sites that lie on a (110) plane. The name "extended" refers to the fact that in this configuration the interstitial is highly delocalized. It has been observed to appear during recrystallization from a planar crystal-amorphous interface in MD simulations.[38] Figure 2(d) shows an interstitial configuration that, to our knowledge, has not yet been reported in the literature. It consists of three displaced atoms and two empty lattice sites. As we shall see, it appears as the saddle

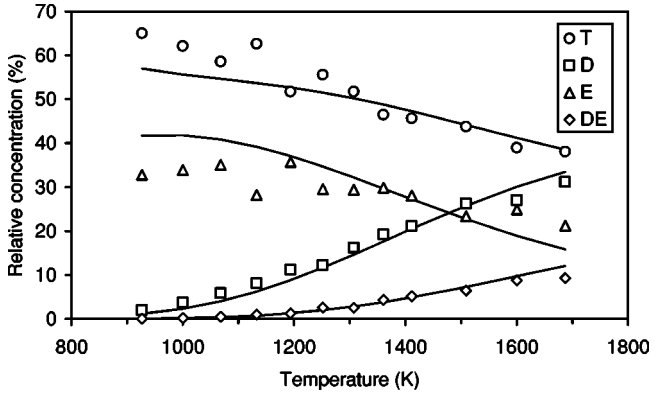

FIG. 3. Relative concentrations of each interstitial configuration as a function of temperature. Symbols are obtained directly from our simulations. Lines represent theoretical fits as obtained from Eqs. (6) and (8) (explanation in text).

point between the D and E configurations. Consequently, we will refer to it as *DE interstitial*. It is worth noting that while the T, D, and E interstitials are high-symmetry configurations, that is not the case of the DE interstitial. A highly asymmetric configuration for the Si self-interstitial was also identified in first-principle calculations,[21] the so-called *caged interstitial*, though with a different geometry. This caged interstitial has been found to be metastable.[13,22]

All these configurations for the Si self-interstitial represent local minima in the potential energy curve, as we have verified by cooling down to 0 K. We have observed that in the case of the T, D, and DE interstitials, small variations in the positions of the atoms around the defect drive to slightly different associated potential energies. Moreover, we have observed that the D and DE configurations represent very shallow potential minima, since slight thermal agitation leads to their transformation to the T and E interstitials. Other interstitial configurations, such as the hexagonal and bond-centered, although also representing local minima in the T3 potential energy curve,[30,33] have not been observed in our dynamic simulations. Symbols in Fig. 3 represent the relative probability of finding the interstitial in a given configuration i as a function of temperature, as obtained in our simulations. These values can be assimilated to the relative concentration of each interstitial species, c^i. As it can be seen, relative concentrations of the T and E interstitials decrease with temperature, while for the D and DE interstitials the concentrations increase. As it can be deduced from Fig. 3, the most frequent configuration is the T interstitial at all simulated temperatures.

Formation enthalpies H^i for each interstitial type i are calculated by the evaluation of the potential energy of the system containing a given configuration and subtracting that of a perfect crystal with the same number of atoms.[33,34] The potential energy corresponding to a perfect crystal lattice at each temperature is extracted by carrying out the same type of time average done for the system with the extra atom. As we have mentioned in the preceding paragraph, small variations in the positions of the atoms involved in the defect produce slightly different values of the potential energy per atom. As an example, we show in Fig. 4 the distribution of

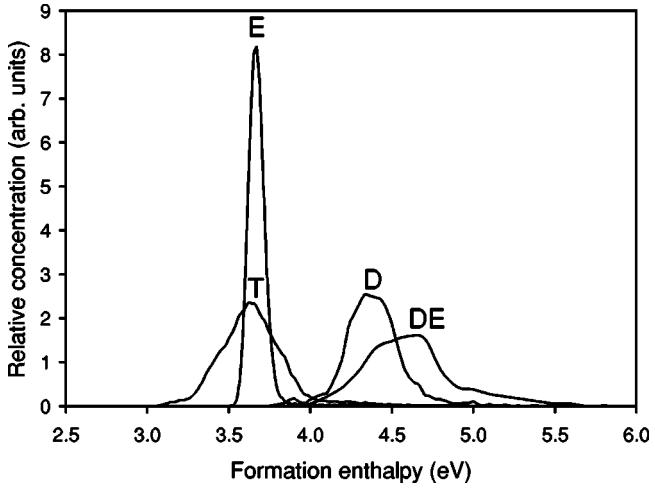

FIG. 4. Formation enthalpy distributions for each interstitial configuration as obtained from simulations at 930 K.

the formation enthalpies corresponding to each interstitial configuration as obtained along the MD simulation at 930 K. While the distribution for the E interstitial is relatively narrow, distributions for the T, D, and DE configurations are wider with an energy spreading of around 1 eV. The peak values corresponding to each distribution were taken as the formation enthalpies for each configuration at 930 K. The formation enthalpies obtained using this criterion at every simulated temperature are represented in Fig. 5. As can be seen, formation enthalpies decrease with temperature, except for the case of the T interstitial where it increases. This trend for the T configuration was also observed by Ungar *et al.* within the MC simulation technique framework.[33] The absolute values they obtained for the formation enthalpy are in good agreement with our results, specially in the low-temperature end. For higher temperatures there is some discrepancy but within their error bars. Lines in Fig. 5 represent best linear fits to the data. It is noteworthy that when ex-

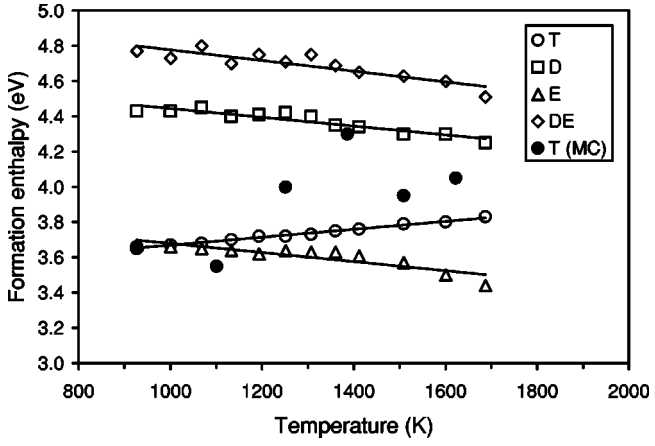

FIG. 5. Formation enthalpies obtained in our simulations for each interstitial configuration as a function of temperature. Values correspond to the peaks in the formation enthalpy distributions for each configuration and temperature. Closed circles represent the MC results for the T interstitial from Ref. 33. Solid lines are best linear fits.

TABLE I. Formation enthalpies (in eV) for several Si self-interstitial configurations as found in the literature. These values have been obtained using different calculation methods, such as relaxation techniques, MD, or MC. The last column shows our results, obtained by extrapolating to 0 K the linear fits of Fig. 5.

Configuration	First principles	Tight binding	Stillinger-Weber	Tersoff 3	This work
T	5.40 (Ref. 51)[a]	3.75 (Ref. 26)	4.84 (Ref. 32)	3.42 (Ref. 33)	3.45
		4.3 (Ref. 25)	4.95 (Ref. 30)	3.45 (Ref. 42)	
		4.39 (Ref. 12)	5.25 (Ref. 42)	3.8 (Ref. 40)	
		4.41 (Ref. 24)	5.28 (Ref. 36)		
		8.10 (Ref. 27)			
D	2.16 (Ref. 21)	3.80 (Ref. 12)	3.5 (Ref. 35)	4.39 (Ref. 33)	4.70
	3.2 (Ref. 20)	5.55 (Ref. 27)	3.65 (Ref. 34)	4.70 (Ref. 42)	
	3.3 (Ref. 16)		3.9 (Ref. 37)	4.7 (Ref. 40)	
	3.31 (Refs. 13 and 22)		4.68 (Ref. 36)		
	3.40 (Ref. 23)		5.26 (Ref. 30)		
	4.96 (Ref. 51)[a]		5.38 (Ref. 32)		
			5.62 (Ref. 42)		
DE					5.08
E	2.29 (Ref. 21)[b]	8.10 (Ref. 27)[b]	3.66 (Ref. 32)[b]	3.85 (Ref. 38)	3.94
	5.17 (Ref. 51)[a,b]		3.7 (Ref. 37)		
			3.76 (Ref. 5)		
			3.91 (Ref. 36)		
Hexagonal	3.31 (Refs. 13 and 22)	3.81 (Ref. 26)	6.54 (Ref. 30)	4.58 (Ref. 33)	
	3.45 (Ref. 23)	4.93 (Ref. 12)	6.58 (Ref. 32)	4.61 (Ref. 42)	
	4.82 (Ref. 51)[a]	5.93 (Ref. 24)	6.95 (Ref. 42)	4.7 (Ref. 40)	
			6.96 (Ref. 36)		
Bond centered			5.61 (Ref. 30)	4.12 (Ref. 33)	
			5.67 (Ref. 32)	5.86 (Ref. 42)	
			5.99 (Ref. 42)	5.9 (Ref. 40)	
			6.00 (Ref. 36)		

[a]Values from Ref. 51 were obtained by fixed-node diffusion quantum Monte Carlo methods.

[b]The enthalpy values corresponding to interstitial configurations described in Refs. 21, 51, 27, and 32 are shown in line E since in the literature are usually considered as "extended," though they are morphologically different from the described E interstitial.

trapolating these lines to $T=0$ K, the formation enthalpy values coincide exactly with the ones obtained by Balamane and co-workers also using MC techniques with the T3 potential for the interstitials T (3.45 eV) and D (4.70 eV).[42] A good agreement is also found between our extrapolation to 0 K for the E interstitial (3.94 eV) and the formation energy calculated by Nishihira and Motooka for the same configuration (3.85 eV).[38] This shows the consistency of our results, and supports the idea of a linear behavior of the enthalpies on T from $T=0$ K up to the melting point. These formation enthalpy values at 0 K, and the ones obtained by other authors using different calculation techniques, are represented in Table I. Energy values for the hexagonal and bond-centered configurations, although not obtained in our simulations, are also shown for the shake of completeness.

From our results it is clear that the lowest formation enthalpy configuration depends on temperature: T below 1000 K and E above. In the case of the SW potential, there are discrepancies: some authors affirm that the lowest formation enthalpy configuration is the T interstitial with 4.95 eV,[30] other authors conclude that it is the D configuration with 3.5–3.7 eV,[34,35] and others the E configuration with 3.6–3.9 eV.[5,32,36,37] This situation is not different within the first-principle framework: most authors coincide that the lowest-energy configuration is the D interstitial, with 2.2–3.4 eV,[16,20,21,23] while Needs[22] and Goedecker *et al.*[13] state that D and hexagonal configurations are degenerate, both having a formation energy of 3.31 eV. However, it is worth noting that, to our knowledge, no *ab initio* calculations have been carried out on the E configuration, although the existence of a delocalized interstitial has been hypothesized within this framework[17] and, in fact, the caged configuration[21] has been described as "extended."[51] In the case of TB simulations, Tang and co-workers[12] found that the lowest-formation-energy configuration is the D interstitial with 3.8 eV. That was the same conclusion for Munro and Wales, but with a higher value for the formation energy, 5.55 eV.[27] In the previous studies of Wang *et al.*[24] and Song *et al.*[25] the D configuration was not considered, only the T and hexagonal configurations, having both higher calculated formation energies than those obtained by Tang *et al.* On the other hand, Lenosky and co-workers obtained a lower formation energy for the T interstitial, 3.75 eV, even though in

their study the D configuration was not considered either.[26] After this brief exposition, one realizes that there is no clear agreement in the literature about which interstitial configuration has the lowest formation enthalpy at 0 K. As we shall see, the macroscopic description does not correspond to the lowest-formation-enthalpy configuration, but to an effective behavior that is affected by all of them.

From the formation enthalpy and the relative concentrations other thermodynamical magnitudes can be extracted. The Gibbs free energy of formation for each configuration i can be obtained by thermodynamic integration:

$$G^i/T - G_0^i/T_0 = \int_{T_0}^{T} -\frac{H^i(\tau)}{\tau^2} d\tau, \tag{5}$$

where G_0^i is a reference free energy value at a given temperature T_0. By assuming a linear dependence of H^i on T, $H^i = a^i T + b^i$, the integration leads to

$$G^i = -a^i T \ln T + \left(\frac{a^i T_0 \ln T_0 + G_0^i - b^i}{T_0} \right) T + b^i. \tag{6}$$

Using the reference value G_0^T for the T interstitial obtained by Ungar *et al.* (3.429 eV at $T_{T3}=500$ K),[33] the Gibbs free energy of formation for the T interstitial, G^T, can be easily obtained from Eq. (6). Once G^T is known, the absolute concentration of this interstitial can be calculated from

$$C^T = C_0 \exp(-G^T/k_B T), \tag{7}$$

where $C_0 = 5 \times 10^{22}$ cm^{-3}, the atomic density of Si. Since we have extracted from our simulations the relative concentrations c^i for each interstitial configuration, we can calculate the Gibbs free energy of formation for the D, E, and DE interstitials by applying

$$G^i = G^T - k_B T \ln(c^i/c^T). \tag{8}$$

G^i also has to fulfill Eq. (6), G_0^i being the only unknown parameter. This parameter for interstitial configurations D, E, and DE can be determined by fitting to the relative concentrations obtained in our simulations. The results of these fittings are represented by solid lines in Fig. 3. As it can be seen, good agreement is found between our simulation results and the fits, except for the case of configurations T and E in the low-temperature end. This might be due to the fact that, as we shall see, at these low temperatures the jump frequency from configuration T to E is reduced and consequently longer simulation times would be needed in order to further improve the statistics. The obtained Gibbs free energies are represented in Fig. 6 as a function of temperature.

The entropies of formation for each configuration can be estimated from the Gibbs free energies and enthalpies:

$$S^i = (H^i - G^i)/T, \tag{9}$$

which are also represented in Fig. 6. As it can be seen, T and E are low-formation-entropy configurations $[(4-6)k_B]$, while D and DE are high-formation-entropy configurations $[(10-13)k_B]$, which is compatible with their increased concentration at higher temperatures. These values compare very well with those estimated using *ab initio* techniques $[(6-10)k_B]$,[16,18] TB calculations $(11.2k_B)$,[12,28] and the SW potential in both MC and MD simulations $[(5-8)k_B]$.[32,35]

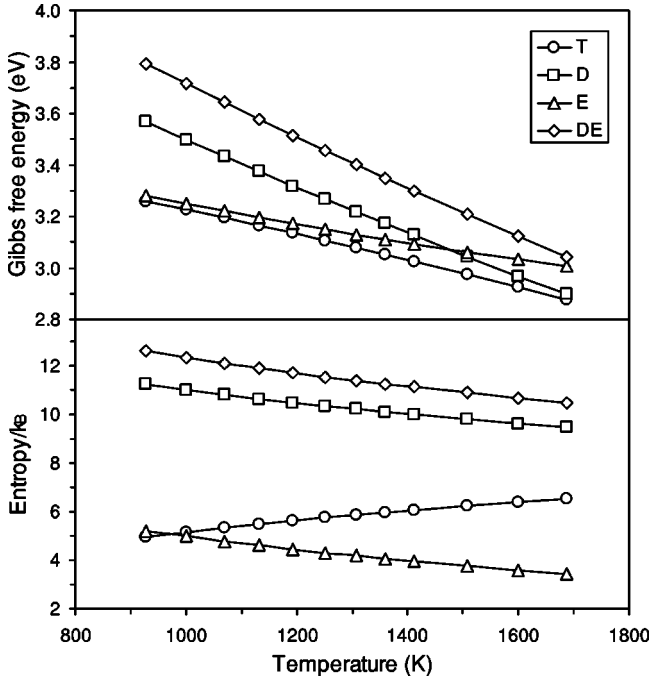

FIG. 6. Gibbs free energies and entropies of formation for each interstitial configuration as a function of temperature.

From the Gibbs free energies we have calculated the absolute concentration of each interstitial configuration the same way we did for the T interstitial by applying Eq. (7). These concentrations are plotted in Fig. 7 as a function of temperature. The summation of all of them gives the total interstitial concentration C predicted by the T3 potential, which is also shown in Fig. 7. Results from other authors using different simulation techniques are also shown. As it can be seen, T3 gives a lower total Si self-interstitial concentration than that predicted by more fundamental methods.

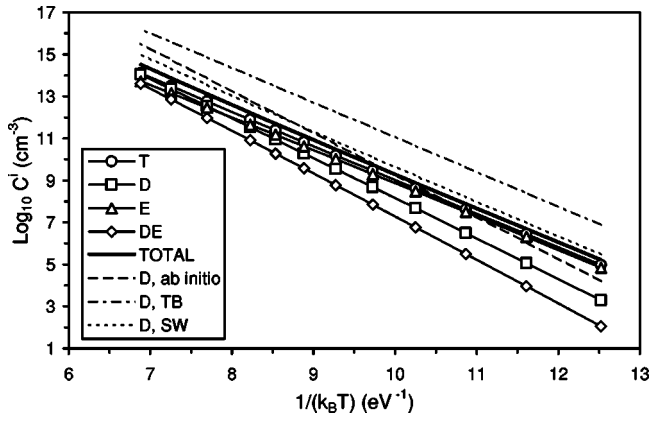

FIG. 7. Absolute concentrations for each interstitial configuration as a function of temperature. The thick solid line represents the total interstitial concentration. The dashed line represents *ab initio* results from Ref. 23, the dashed-dotted line TB results from Ref. 12, and the dotted line MD results using the SW potential from Ref. 35, where only configuration D was considered.

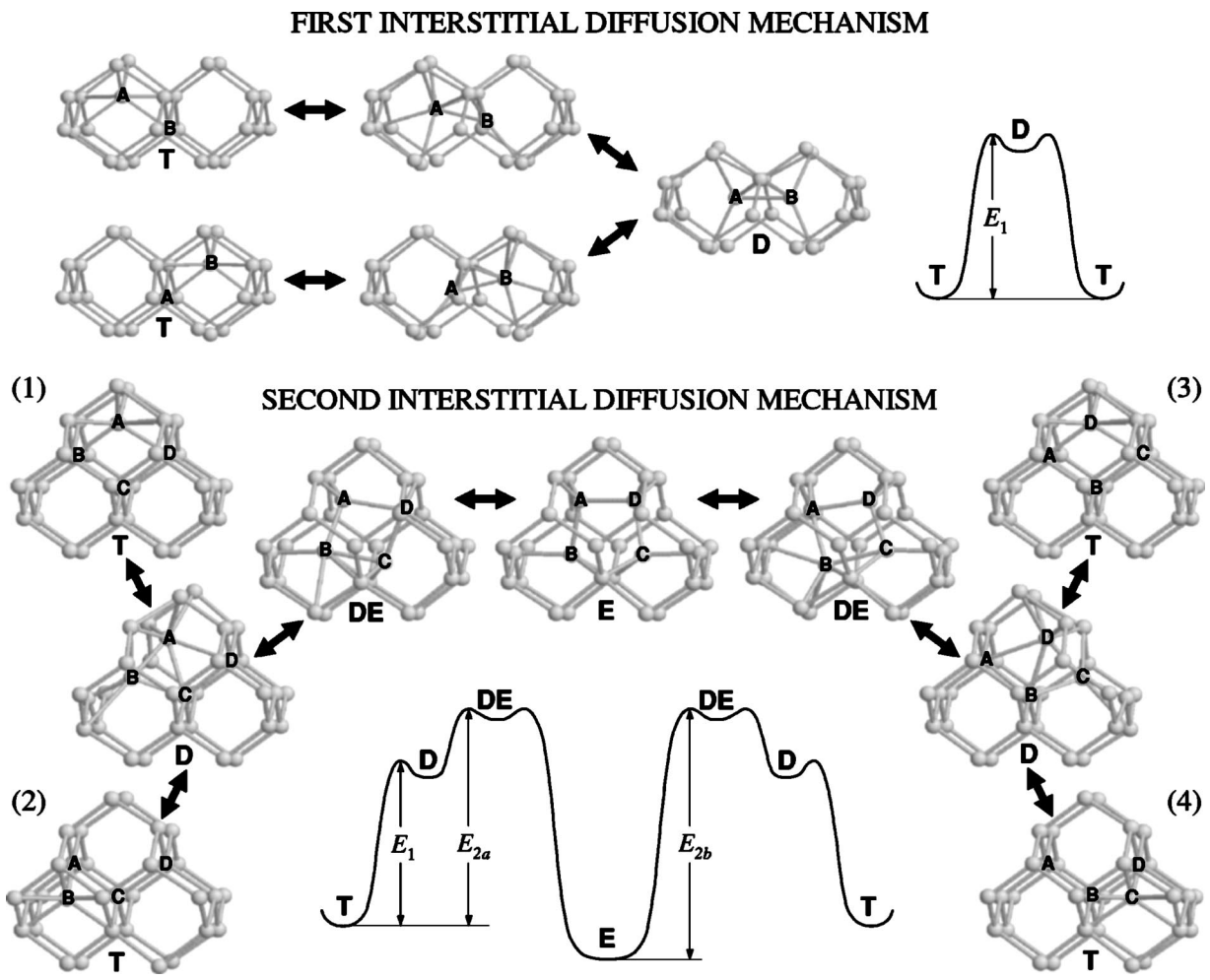

FIG. 8. The two interstitial diffusion mechanisms identified in our simulations. In the first one the D configuration is the saddle point between two neighboring tetrahedral sites. In the second mechanism the configuration changes from T to E going through two saddle points, which are the D and DE interstitials. Energy diagrams for each diffusion mechanism are also shown.

The total Si self-interstitial concentration is fitted very well to an Arrhenius dependence, given by

$$C = 8.31 \times 10^{25} \exp\left(-\frac{3.83\ \text{eV}}{k_B T}\right) \text{cm}^{-3}. \qquad (10)$$

It is interesting to note that, in spite of the contribution of different interstitial configurations, and the variation of their corresponding formation enthalpies and entropies with temperature, the total Si self-interstitial concentration can still be described by a pure Arrhenius behavior with a single activation energy. Since the prefactor is 1662 times higher than the normalized C_0, Eq. (10) can be rewritten with C_0 as the prefactor by introducing a linear dependence with T in the exponential:

$$C = 5 \times 10^{22} \exp\left(-\frac{3.83 - 7.42 k_B T}{k_B T}\right) \text{cm}^{-3}. \qquad (11)$$

The expression inside the exponential can be assigned to an *effective* Si self-interstitial Gibbs free energy, G. The fact that G is linear with T implies that the effective entropy, $S = -\partial G/\partial T|_P$, is constant, and so is the effective enthalpy H. Then, 3.83 eV corresponds to H, and $7.42 k_B$ to S. These values are intermediate to those obtained for the different interstitial configurations. In the light of this analysis, it is remarkable that macroscopic behavior can be described in terms of a unique effective interstitial configuration with constant formation enthalpy and entropy. These effective values would be related to experimental measurable magnitudes, but do not correspond to any of the theoretically determined individual interstitial configurations.

B. Si self-interstitial diffusivity

We have observed that the change in time of the Si self-interstitial configuration is correlated with the interstitial diffusion process. We have identified two different diffusion mechanisms, which are both sketched in Fig. 8, along with the corresponding energy diagrams. In the first one, the interstitial moves between two neighboring tetrahedral sites, the D configuration being the saddle point in the transition. In the second mechanism, the interstitial configuration changes between T and E going through two saddle points, which are the D and the DE configurations. In this second

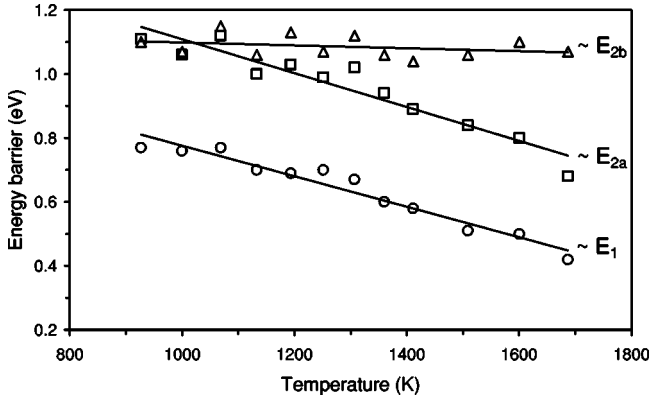

FIG. 9. Energy barrier estimations for the two interstitial diffusion mechanisms shown in Fig. 8 as a function of temperature. Solid lines are best linear fits.

mechanism, when going from (1) to (3) there is no net diffusion, just an orbital atomic motion where atoms *A*, *B*, *C*, and *D* exchange their positions. The first diffusion mechanism has also been observed in TB calculations,[12] but with configuration T being the saddle point in the transition instead of configuration D. This is also the case in some of the MD simulations using the SW potential.[34,35] However, in other MD studies also using the SW potential the diffusion is described by a jump-rotation mechanism involving primarily the D configuration.[36] Maroudas and Brown, using MC techniques with the SW potential, have proposed that interstitial self-diffusion happens between two nearest-neighbor tetrahedral sites going through the intermediate hexagonal site.[31] In first-principle calculations the D configuration has been also given a fundamental role in the interstitial-mediated diffusion mechanism, but through a different migration path involving the caged configuration[21] or the hexagonal configuration.[22] On the other hand, the transition between D and E configurations has also been observed in MD simulations using the SW (Refs. 36 and 37) and T3 (Ref. 38) potentials, but in this last case with a rather complex transition path involving six intermediate configurations.

Given the mechanisms and energetics shown in Fig. 8, and taking into account that configurations D and DE are very shallow potential energy minima, the energy barriers for diffusion can be assimilated in a first approximation to the formation enthalpy differences between the interstitial configurations: $E_1 \sim H^D - H^T$, $E_{2a} \sim H^{DE} - H^T$, and $E_{2b} \sim H^{DE} - H^E$. Since these energies vary linearly with temperature, as shown in Fig. 5, so their differences do too. These differences are represented in Fig. 9 as a function of temperature. As can be seen, E_1 is lower than E_{2a} for all the temperature interval considered in our study, which gives an indication that the interstitial diffusion process is dominated by the first proposed mechanism. Occasionally, when the E_{2a} barrier is overcome the system gets to configuration E. The time it stays there should be rather long since the barrier E_{2b} (from E to DE) that has to be overcome to get back to the T configuration is high.

To quantify the interstitial diffusion process we have calculated the summation of the squared displacements (SD) over all atoms in the simulation cell:

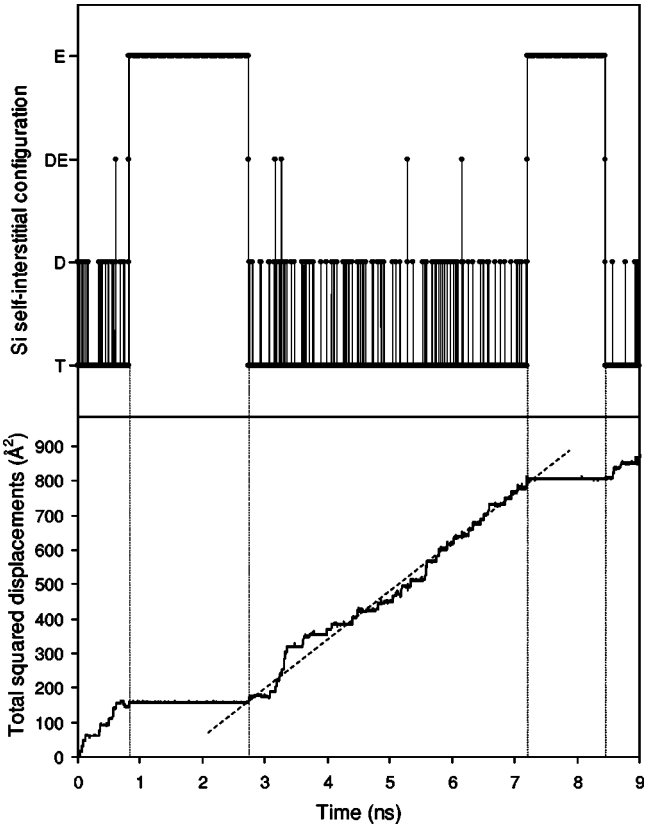

FIG. 10. Time evolution of the interstitial configuration (upper) and the total squared atomic displacements SD (lower) during the first 9 ns of the MD simulation at 930 K. There is a clear correlation between the change in the interstitial configuration and the diffusion process. The dashed line represents the slope in SD associated with interstitial diffusion through mechanism one.

$$\mathrm{SD} = \sum_i [\vec{r}_i(t) - \vec{r}_i(0)]^2 \tag{12}$$

In Fig. 10 we show the evolution in time of both the interstitial configuration and SD during the first 9 ns of the simulation carried out at 930 K. Some useful information can be extracted from the inspection of that figure, which confirms the indications given in the preceding paragraph and deduced from the energy diagrams. First, SD remains constant while the interstitial configuration is T or E. Second, when the interstitial gets to configuration E, the time it stays there is significantly much larger than when staying in the T configuration. Third, the increase in SD occurs mainly when the interstitial switches its configuration between T and D (mechanism one).

The Einstein formula relates the diffusion coefficient *d* with SD:

$$d = \lim_{t\to\infty} \frac{1}{6t} \sum_i [\vec{r}_i(t) - \vec{r}_i(0)]^2 = \lim_{t\to\infty} \frac{\mathrm{SD}(t)}{6t}. \tag{13}$$

By applying the formula, *d* can be extracted from the slope of the SD(*t*) curve for each simulated temperature. Even though thermal agitation has been eliminated by the time average of the atom positions, simulation times have to be

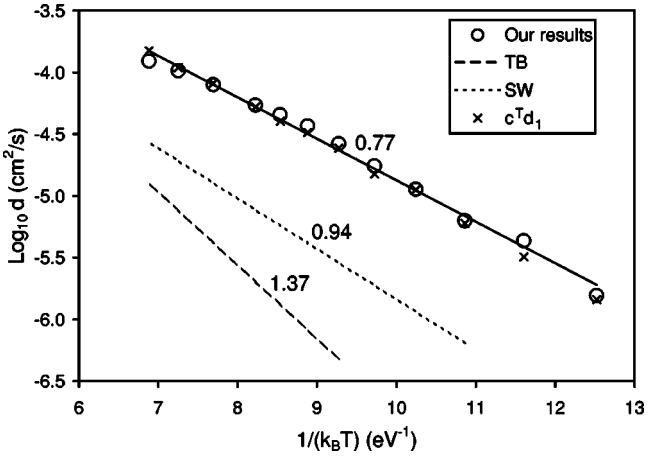

FIG. 11. Arrhenius plot of the interstitial diffusion coefficients. Open circles represent our results obtained by a linear fit to the SD versus time curves for each temperature. We show as well results from other authors: the dotted line is from Sinno *et al.* who used the SW potential (Ref. 35), and the dashed line represents TB data by Tang *et al.* (Ref. 12). Next to each line we have indicated the corresponding activation energy (in eV). Crosses represent the contribution to diffusion of the first mechanism.

long enough to saturate orbital motion like that previously mentioned, and to compensate for the enhanced stability of the E configuration, above all at low temperatures. For instance, to get a reliable slope in SD(t) for the lowest simulated temperature (930 K) we had to run the simulation for 1.6×10^8 time steps (equivalent to a simulated time of one tenth of a microsecond), rather long for the MD standard.

In Fig. 11 we have plotted the interstitial diffusion coefficients we have extracted from our simulations. The fit of our results to an Arrhenius plot gives a prefactor of 3.04×10^{-2} $\mathrm{cm^2/s}$ and an activation energy of 0.77 eV. In the literature, apart from a few exceptions,[22,31] activation energies for interstitial-mediated diffusion have been determined to be between 0.65 and 1.37 eV.[12,29,34–37] For the sake of comparison, we have chosen to represent in Fig. 11 results from other authors obtained using the SW potential[35] and TB techniques,[12] some of the more representative from the literature. As it can be seen, our simulations predict a higher mobility for the Si self-interstitial than the SW and TB calculations. The bigger discrepancy with respect to the activation energy is with the TB results from Tang *et al.* However, very recent calculations also using TB techniques determine an activation energy for Si self-interstitial diffusion of 0.8 eV,[29] much closer to our results.

From the preceding analysis it seems that interstitial-mediated diffusion is dominated by the first mechanism. The relative contribution to diffusion of the different mechanisms can be calculated by applying the following expression,

$$d = \sum_i c^i d_i \tag{14}$$

which relates the interstitial diffusion coefficient d with the diffusivity d_i associated with each different mechanism and the relative concentration c^i of the main diffusing species. The diffusion coefficient associated with the first proposed mechanism, d_1, can be calculated at each temperature from the slope of SD(t) in the time intervals where only the first mechanism is operative, which are easily identified as can be seen in Fig. 10. By fitting the extracted d_1 values to an Arrhenius plot we have determined that this mechanism contributes as

$$d_1 = 2.16\times10^{-1}\exp\left(-\frac{0.92\ \mathrm{eV}}{k_B T}\right)\mathrm{cm^2/s}. \tag{15}$$

In Fig. 11 we have represented the product $c^T d_1$, where c^T is the relative concentration of configuration T (plotted in Fig. 3), the main diffusing species of mechanism one. As it can be seen, the product $c^T d_1$ coincides with the diffusion coefficient obtained from the MD simulations. This is the confirmation that effectively, interstitial diffusion is dominated by the first proposed mechanism, the second mechanism only acting as a delayer of the diffusion process. When the system gets to configuration E diffusion stops for a while, as it was shown in Fig. 10. The time the system stays in configuration E is rather long, or equivalently its relative concentration is high. Consequently, the relative concentration of the diffusive configuration T is reduced. This result also shows that even though diffusion is determined by mechanism one, the activation energy for diffusion does not coincide with 0.92 eV, due to the contribution of the relative concentration of configuration T, which decreases with temperature (negative activation energy). This finding indicates that if diffusion can take place through several mechanisms, the energy barrier associated with the saddle point of the dominant one is not necessarily the activation energy of the diffusion process. Differences also occur with the prefactor of the effective diffusion coefficient, which is about one order of magnitude lower than that of d_1. Generally, prefactors larger than those corresponding to the vibrational frequency of the Si crystal are associated with entropy contributions.[52] This study provides a physical explanation for smaller effective prefactors when the relative concentration of the diffusive species is much less than unity. If configurations involved in mechanisms of negligible diffusivity are fairly stable, their relative concentration could be high enough (therefore the relative concentration of the diffusing species would be low) to significantly reduce the effective diffusion coefficient.

The interstitial self-diffusion coefficient D can be calculated from the normalized interstitial concentration c (the total interstitial concentration C shown in Fig. 7 divided by C_0) and the interstitial diffusion coefficient d:

$$D = cd \tag{16}$$

Experiments in isotope heterostructures have shown that self-diffusivity in Si follows an Arrhenius behavior over a wide temperature range.[9] Even though results from self-diffusion studies are generally not easily separable into the individual mechanisms, the interstitial contribution to self-diffusion in Si has been estimated from metal diffusion experiments[8] and by inverse modeling of the Ostwall ripening process of {113} defects.[10] These experimental findings are plotted in Fig. 12 along with our own simulation results

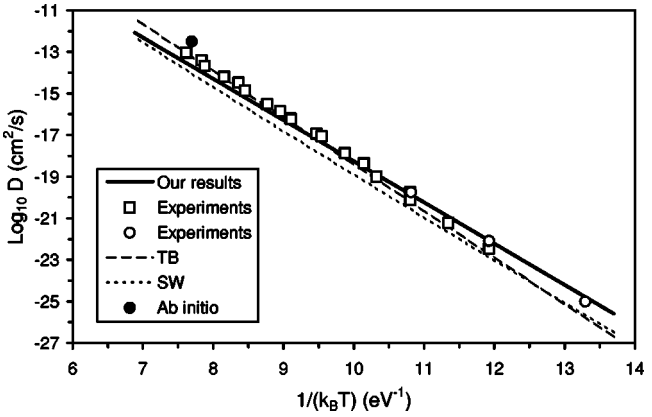

FIG. 12. Arrhenius plot of the interstitial self-diffusion coefficients. The thick solid line represents our results. We show as well experimental measurements from Ref. 8 and Ref. 10 (open squares and circles, respectively), TB results from Ref. 28, MD results using the SW potential from Ref. 35, and *ab initio* results from Ref. 16.

and the ones obtained by other authors using different simulation techniques. The fitting to an Arrhenius plot gives a prefactor of 52.89 cm^2/s and an activation energy of 4.60 eV. Agreement with experiments is quite good, apart from minor differences that may be a consequence of neglecting the influence of charged species in the diffusion process. Nevertheless, this agreement is better than the one achieved by the SW potential at all temperatures and, in relation to TB results, ours are closer to experiments in the low-temperature end. It is noteworthy that despite the complex microscopic description of the Si self-interstitial, and the existence of two different diffusion mechanisms whose associated energy barriers change with temperature, the interstitial self-diffusion coefficient still follows an Arrhenius behavior for the full simulated temperature range.

V. CONCLUSIONS

We have studied the interstitial contribution to self-diffusion in Si using classical MD simulation techniques within the T3 description of the atomic interaction forces. In order to compare with experiments and simulation results from other authors, we have introduced a scaling law between real temperatures and Tersoff 3 temperatures. To analyze our simulation results we have used a method based on the time average of the atom coordinates. This allows the direct extraction of the configuration and energetics of the Si self-interstitial as a function of time and temperature. Since our simulations are fully dynamic, no restriction has been posed on interstitial configurations and diffusion paths. We have identified four basic interstitial configurations, T, D, E and DE, and determined their relative concentrations and formation enthalpies. From these results, and by the use of thermodynamic integration techniques, we have calculated other magnitudes such as the Gibbs free energies and entropies of formation, and the absolute concentration for each configuration as a function of temperature. By monitoring the time evolution of the Si self-interstitial configuration and its correlation with the mean square displacement, we have identified two diffusion mechanisms. In the dominant one, the interstitial moves between two tetrahedral sites trough a saddle point represented by the D configuration. In the second diffusion mechanism, the interstitial configuration changes from T to E going through two saddle points, which are D and DE configurations.

General good agreement is found between our results and the ones obtained by other authors using different simulation techniques. One of the differences of our results with respect to TB and classical MD studies using the SW potential is that the role of T and D configurations appears to be exchanged. However, since the energy values corresponding to the lowest-energy and saddle point configurations are approximately the same, the description of the microstructural evolution of the Si lattice during interstitial self-diffusion is the same. The other difference with respect to TB and SW results lies in the individual contributions of *c* and *d*, which are higher and lower than our results, respectively. However, the product of the two contributions is comparable in all cases, and agree very well with experiments. The predicted activation energy for interstitial-mediated self-diffusion is of 4.60 eV for the full simulated temperature interval. With respect to first-principle results, the discrepancy is bigger. While the T3 model predicts that the T interstitial is the lowest in energy, first-principle calculations show that this is not a stable configuration. On the other hand, *ab initio* studies find a stable hexagonal defect that is very low in energy, while in our dynamic simulations that configuration is found to be unstable. Consequently, it is important to remark that the validity of the stable configurations and diffusion mechanisms described in the present study should be considered just within the T3 model of Si.

In our simulations we have found that the interstitial diffusion process involves a rather complex microscopic description: the lowest-energy Si self-interstitial configuration depends on temperature, there are two different interstitial diffusion mechanisms, and the saddle-point energy of the dominant one also changes with temperature. However, the macroscopic behavior can be modeled by a simple description based on a unique interstitial species with an effective formation enthalpy of 3.83 eV and a migration barrier of 0.77 eV. The exact numbers do not correspond to any of the individual interstitial configurations or diffusion mechanisms, but they are the result of the *averaged* behavior of all of them. These findings help to explain why it is not straightforward to justify the experimental measurements on interstitial diffusion, related to the macroscopic behavior, resorting to a particular interstitial configuration and diffusion path theoretically determined.

ACKNOWLEDGMENTS

This work has been supported by the Spanish DGICYT under Project No. BFM 2001-2250 and the JCYL Consejería de Educación y Cultura under Project No. VA-010/02.

[1] P. M. Fahey, P. B. Griffin, and J. D. Plummer, Rev. Mod. Phys. **61**, 289 (1989).
[2] M. Jaraiz, L. Pelaz, E. Rubio, J. Barbolla, G. H. Gilmer, D. J. Eaglesham, H. J. Gossmann, and J. M. Poate, Mater. Res. Soc. Symp. Proc. **54**, 532 (1998).
[3] S. Takeda, M. Kohyama, and K. Ibe, Philos. Mag. A **70**, 287 (1994).
[4] A. E. Michel, W. Rausch, P. A. Ronsheim, and R. H. Kastl, Appl. Phys. Lett. **50**, 416 (1987).
[5] H. R. Schober, Phys. Rev. B **39**, 13 013 (1989).
[6] D. Maroudas and S. T. Pantelides, Chem. Eng. Sci. **49**, 3001 (1994).
[7] T. Y. Tan and U. Gösele, Appl. Phys. A: Solids Surf. **37**, 1 (1985).
[8] H. Bracht, N. A. Stolwijk, and H. Mehrer, Phys. Rev. B **52**, 16 542 (1995).
[9] H. Bracht, E. E. Haller, and R. Clark-Phelps, Phys. Rev. Lett. **81**, 393 (1998).
[10] N. E. B. Cowern, G. Mannino, P. A. Stolk, F. Roozeboom, H. G. A. Huizing, J. H. M. van Berkum, F. Cristiano, A. Claverie, and M. Jaraiz, Mater. Sci. Semicond. Process. **2**, 369 (1999).
[11] K. C. Pandey, Phys. Rev. Lett. **57**, 2287 (1986).
[12] M. Tang, L. Colombo, J. Zhu, and T. D. de la Rubia, Phys. Rev. B **55**, 14 279 (1997).
[13] S. Goedecker, T. Deutsch, and L. Billard, Phys. Rev. Lett. **88**, 235501 (2002).
[14] L. A. Marqués, L. Pelaz, J. Hernández, J. Barbolla, and G. H. Gilmer, Phys. Rev. B **64**, 045214 (2001).
[15] L. A. Marqués, L. Pelaz, M. Aboy, L. Enríquez, and J. Barbolla, Phys. Rev. Lett. **91**, 135504 (2003).
[16] P. E. Blöchl, E. Smargiassi, R. Car, D. B. Laks, W. Andreoni, and S. T. Pantelides, Phys. Rev. Lett. **70**, 2435 (1993).
[17] R. Car, P. J. Kelly, A. Oshiyama, and S. T. Pantelides, Phys. Rev. Lett. **52**, 1814 (1984).
[18] R. Car, P. Blöchl, and E. Smargiassi, Mater. Sci. Forum **83–87**, 433 (1992).
[19] J. Zhu, L. H. Yang, C. Mailhiot, T. D. de la Rubia, and G. H. Gilmer, Nucl. Instrum. Methods Phys. Res. B **102**, 29 (1995).
[20] J. Zhu, T. D. de la Rubia, L. H. Yang, C. Mailhiot, and G. H. Gilmer, Phys. Rev. B **54**, 4741 (1996).
[21] S. J. Clark and G. J. Ackland, Phys. Rev. B **56**, 47 (1997).
[22] R. J. Needs, J. Phys.: Condens. Matter **11**, 10437 (1999).
[23] O. K. Al-Mushadani and R. J. Needs, Phys. Rev. B **68**, 235205 (2003).
[24] C. Z. Wang, C. T. Chan, and K. M. Ho, Phys. Rev. Lett. **66**, 189 (1991).
[25] E. G. Song, E. Kim, Y. H. Lee, and Y. G. Hwang, Phys. Rev. B **48**, 1486 (1993).
[26] T. J. Lenosky, J. D. Kress, I. Kwon, A. F. Voter, B. Edwards, D. F. Richards, S. Yang, and J. B. Adams, Phys. Rev. B **55**, 1528 (1997).
[27] L. J. Munro and D. J. Wales, Phys. Rev. B **59**, 3969 (1999).
[28] A. Jääskeläinen, L. Colombo, and R. Nieminen, Phys. Rev. B **64**, 233203 (2001).
[29] D. A. Richie, J. Kim, S. A. Barr, K. R. A. Hazzard, R. Hennig, and J. W. Wilkins, Phys. Rev. Lett. **92**, 045501 (2004).
[30] I. P. Batra, F. F. Abraham, and S. Ciraci, Phys. Rev. B **35**, 9552 (1987).
[31] D. Maroudas and R. A. Brown, Appl. Phys. Lett. **62**, 172 (1993).
[32] D. Maroudas and R. A. Brown, Phys. Rev. B **47**, 15 562 (1993).
[33] P. J. Ungar, T. Halicioglu, and W. A. Tiller, Phys. Rev. B **50**, 7344 (1994).
[34] G. H. Gilmer, T. D. de la Rubia, D. M. Stock, and M. Jaraiz, Nucl. Instrum. Methods Phys. Res. B **102**, 247 (1995).
[35] T. Sinno, K. Jiang, and R. A. Brown, Appl. Phys. Lett. **68**, 3028 (1996).
[36] M. Nastar, V. V. Bulatov, and S. Yip, Phys. Rev. B **53**, 13 521 (1996).
[37] M. Hane, T. Ikezawa, and A. Furukawa, IEICE Trans. Electron. **E83-C**, 1247 (2000).
[38] K. Nishihira and T. Motooka, Phys. Rev. B **66**, 233310 (2002).
[39] F. H. Stillinger and T. A. Weber, Phys. Rev. B **31**, 5262 (1985).
[40] J. Tersoff, Phys. Rev. B **38**, 9902 (1988).
[41] J. M. Haile, *Molecular Dynamics Simulations: Elementary Methods* (Wiley, New York, 1992).
[42] H. Balamane, T. Halicioglu, and W. A. Tiller, Phys. Rev. B **46**, 2250 (1992).
[43] J. W. Mayer and S. S. Lau, *Electronics Materials Science for Integrated Circuits in Si and GaAs* (MacMillan, New York, 1990).
[44] L. J. Porter, S. Yip, M. Yamaguchi, H. Kaburaki, and M. Tang, J. Appl. Phys. **81**, 96 (1997).
[45] C. W. Gear, *Numerical Initial Value Problems in Ordinary Differential Equations* (Prentice-Hall, New Jersey, 1971).
[46] H. Jónsson, G. Mills, and K. W. Jacobsen, *Classical and Quantum Dynamics in Condensed Phase Simulations* (World Scientific, Singapore, 1998).
[47] R. Elber and M. Karplus, Chem. Phys. Lett. **139**, 375 (1987).
[48] Y. Song, R. Malek, and N. Mousseau, Phys. Rev. B **62**, 15 680 (2000).
[49] L. A. Marqués, M.-J. Caturla, T. D. de la Rubia, and G. H. Gilmer, J. Appl. Phys. **80**, 6160 (1996).
[50] M.-J. Caturla, T. D. de la Rubia, L. A. Marqués, and G. H. Gilmer, Phys. Rev. B **54**, 16 683 (1996).
[51] W.-K. Leung, R. J. Needs, G. Rajagopal, S. Itoh, and S. Ihara, Phys. Rev. Lett. **83**, 2351 (1999).
[52] B. I. Boltaks, *Diffusion in Semiconductors* (Academic Press, New York, 1963).